J Pediatr (Rio J). 2019;95(6):674–681

Jornal de Pediatria

www.jped.com.br

ORIGINAL ARTICLE

Radiographic predictors determined with an objective assessment tool for neonatal patients with necrotizing enterocolitis☆

Allan Felipe Fattori Alves [a,1], Ana Luiza Menegatti Pavan [a,1], Guilherme Giacomini [a], Caio Cesar Quini [a], Sergio Marrone Ribeiro [b], Rozemeire Garcia Marquez [b], Maria Regina Bentlin [b], André Petean Trindade [b], José Ricardo de Arruda Miranda [a], Diana Rodrigues de Pina [b,*]

[a] *Universidade Estadual Paulista (UNESP), Instituto de Biociências de Botucatu (IBB), Botucatu, SP, Brazil*
[b] *Universidade Estadual Paulista (UNESP), Faculdade de Medicina de Botucatu (FMB), Botucatu, SP, Brazil*

Received 25 February 2018; accepted 17 May 2018
Available online 3 July 2018

KEYWORDS
Necrotizing enterocolitis;
Abdominal radiography;
Image processing;
Texture analyses, wavelet

Abstract

Objective: The objective of this study was to develop and validate a computational tool to assist radiological decisions on necrotizing enterocolitis.

Methodology: Patients that exhibited clinical signs and radiographic evidence of Bell's stage 2 or higher were included in the study, resulting in 64 exams. The tool was used to classify localized bowel wall thickening and intestinal pneumatosis using full-width at half-maximum measurements and texture analyses based on wavelet energy decomposition. Radiological findings of suspicious bowel wall thickening and intestinal pneumatosis loops were confirmed by both patient surgery and histopathological analysis. Two experienced radiologists selected an involved bowel and a normal bowel in the same radiography. The full-width at half-maximum and wavelet-based texture feature were then calculated and compared using the Mann–Whitney U test. Specificity, sensibility, positive and negative predictive values were calculated.

Results: The full-width at half-maximum results were significantly different between normal and distended loops (median of 10.30 and 15.13, respectively). Horizontal, vertical, and diagonal wavelet energy measurements were evaluated at eight levels of decomposition. Levels 7 and 8 in the horizontal direction presented significant differences. For level 7, median was 0.034 and 0.088 for normal and intestinal pneumatosis groups, respectively, and for level 8 median was 0.19 and 0.34, respectively.

☆ Please cite this article as: Fattori Alves AF, Menegatti Pavan AL, Giacomini G, Quini CC, Marrone Ribeiro S, Garcia Marquez R, et al. Radiographic predictors determined with an objective assessment tool for neonatal patients with necrotizing enterocolitis. J Pediatr (Rio J). 2019;95:674–81.

* Corresponding author.
E-mail: drpina@fmb.unesp.br (D. R. Pina).

[1] These authors contributed equally to this work.

https://doi.org/10.1016/j.jped.2018.05.017

Conclusions: The developed tool could detect differences in radiographic findings of bowel wall thickening and IP that are difficult to diagnose, demonstrating the its potential in clinical routine. The tool that was developed in the present study may help physicians to investigate suspicious bowel loops, thereby considerably improving diagnosis and clinical decisions.

PALAVRAS-CHAVE
Enterocolite necrotizante;
Radiografia abdominal;
Processamento de imagem;
Análises de textura, *wavelet*

Preditores radiográficos determinados com uso de ferramenta de avaliação objetiva para pacientes neonatais com enterocolite necrotizante

Resumo
Objetivo: O objetivo deste estudo foi desenvolver e validar uma ferramenta computacional para auxiliar as decisões radiológicas na enterocolite necrotizante.
Metodologia: Pacientes que exibiam sinais clínicos e evidências radiográficas do estágio 2 ou superior de Bell foram incluídos no estudo, que resultou em 64 exames. A ferramenta foi usada para classificar o aumento localizado da espessura da parede intestinal e a pneumatose intestinal com medidas de largura total a meia altura e análises de textura baseadas na decomposição da energia *wavelet*. Os achados radiológicos de aumento suspeito da espessura da parede intestinal e das alças na pneumatose intestinal foram confirmados pela cirurgia e análise histopatológica do paciente. Dois radiologistas experientes selecionaram um intestino afetado e um intestino normal na mesma radiografia. A largura total a meia altura e a característica da textura baseada em *wavelet* foram então calculadas e comparadas com o uso do teste U de Mann-Whitney. Foram calculados a especificidade, sensibilidade, valores preditivos positivos e negativos.
Resultados: Os resultados da largura total a meia altura foram significativamente diferentes entre a alça normal e a distendida (mediana de 10,30 e 15,13, respectivamente). Medidas de energia *wavelet* horizontal, vertical e diagonal foram avaliadas em oito níveis de decomposição. Os níveis 7 e 8 na direção horizontal apresentaram diferenças significativas. Para o nível 7, as medianas foram 0,034 e 0,088 para os grupos normal e com pneumatose intestinal, respectivamente, e para o nível 8, as medianas foram 0,19 e 0,34, respectivamente.
Conclusões: A ferramenta desenvolvida pode detectar diferenças nos achados radiográficos do aumento da espessura da parede intestinal e PI de difícil diagnóstico, demonstra seu potencial na rotina clínica. A ferramenta desenvolvida no presente estudo pode ajudar os médicos a investigar alças intestinais suspeitas e melhorar consideravelmente o diagnóstico e as decisões clínicas.

Introduction

Necrotizing enterocolitis (NEC) is one of the most common and unpredictable intestinal disorders that involve systemic inflammatory responses in premature infants.[1–4] The disease affects 1–3% of neonatal intensive care unit admissions.[5] Over the last few decades, NEC has emerged as one of the most common surgical emergencies in neonates, with high morbidity and mortality.[6,7] Advances in neonatal care have increased survival rates among premature infants, with a concomitant increase in the incidence of NEC.[6,8]

NEC is characterized by ischemic necrosis of the gastrointestinal tract that often leads to perforation and peritonitis.[9] The diagnosis and management of NEC are based on clinical signs, symptoms, and findings on abdominal radiographs.[3,4,10,11] Once NEC is suspected, the patient undergoes a regular routine of abdominal radiography[3,10,12] that seeks to follow disease progression and guide clinical management.[3,4,6,11,13] The timing of follow-up abdominal radiographs depends on the severity of NEC and varies from six to 24 h.[12] Such follow-up may indicate the need for surgical intervention.[4,6,13] Radiological signs of NEC include generalized intestinal distension, localized bowel loop distension, bowel wall thickening (BWT), intestinal pneumatosis (IP), air within the portal system, and pneumoperitoneum.[14] However, even with these predictors, the diagnosis of NEC is a very difficult task for physicians.[10,13]

Some studies have been conducted to better understand the etiology of NEC and ways of preventing its progression; however, few have generated significant results that led to changes in clinical practice.[3,15–18] Some infant cases present the disease so acutely and severely that morbidity or mortality cannot be avoided despite treatment. The identification of early signs of the disease may allow more accurate diagnosis and treatment.[3] In the present work, the authors proposed to validate an automatic and objective computational tool to assist the radiologist's decisions in NEC cases. Image processing techniques were applied to radiographs to classify bowel loop involvement.[19] The computational tool was able to classify both BWT and IP using

full-width at half-maximum (FWHM) and texture analyses following wavelet energy decompositions. In addition, this tool can be used as an indicator of disease severity, aiding clinical management and surgical decisions.

Methodology

The validation of a developed semi-automatic tool was proposed in this study to help physicians in the diagnosis of NEC. In this algorithm, the radiologist identifies a suspicious bowel which needs further investigation. The user is asked to select a region of interest (ROI) to be studied and FWHM or wavelet transform are used to extract objective information. Supplementary Fig. 1 contains a flowchart with detailed procedure steps. Further explanations are described in subsections.

Patient selection

The present study retrospectively evaluated newborns who were diagnosed with NEC and treated at Botucatu Medical School, São Paulo State University, Brazil, between 2008 and 2015. All image acquisitions, transfers, manipulation, and processing were compliant with the Committee for Ethics in Human Research regulations of author's institution (protocol No. 55884516.0.0000.5411).

Throughout the entire study the disease stage was determined by two physicians according to modified Bell's staging criteria.[20] These staging criteria are used for clinical classification and management of NEC, in which a composite of clinical signs and symptoms (*e.g.*, abdominal distension, bloody stool, and hypotension), biochemical parameters (*e.g.*, thrombocytopenia and neutropenia), and radiographic signs (*e.g.*, IP and pneumoperitoneum) are used to grade the severity of NEC.[20–22] Eighty radiographs were selected in which NEC was the main suspected disease, and a single radiograph was used per patient. During the analysis or radiographs, radiologists were unaware of the clinical information, the outcome of the surgery, and histopathological analysis.

Patients were admitted to this hospital due to a combination of the following symptoms: apnea, bradycardia, temperature instability, thrombocytopenia, metabolic acidosis, oliguria, hypotension, coagulopathy, shock, grossly bloody stools, prominent abdominal distension, abdominal wall edema, erythema, and induration.

Patients who exhibited clinical signs and radiographic evidence of Bell's stage 2 or higher were included in the study, resulting in 64 exams. Patients were excluded if they presented intra-abdominal congenital anomalies. From the 64 exams included, 50 were submitted to surgery and histopathological analysis. Their gestational age ranged from 23 to 40 weeks (mean gestational age 27 weeks). Forty-three (93.5%) patients were preterm, while the remaining seven (6.5%) newborns were full term. Birth weight ranged from 462 to 3610 g (average weight: 1152 g). There were 38 patients (19.4%) with stage 2 NEC, and 12 patients (6.5%) with stage 3 NEC according to the Bell scoring system.

The dataset was divided into two groups (BWT and IP) after evaluation by two experienced radiologists. The BWT group consisted of 30 radiographs and the IP group consisted of 15 radiographs. For each patient, both normal and abnormal loops were identified inside the same radiographic image.

The identification of normal loops within each patient made it possible to compare them with the abnormal loops.

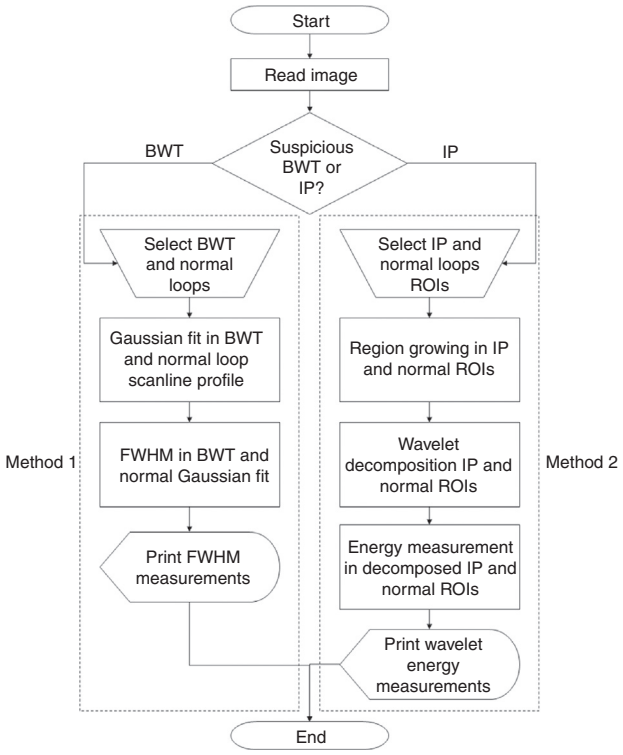

Figure 1 Methodological flowchart for assessing necrotizing enterocolitis in neonatal radiographs. Two different methods are present. Method 1 uses full-width at half-maximum (FWHM) measurements to identify bowel wall thickening (BWT). Method 2 is a hybrid tool which applies region growing, wavelet transform, and energy measurement to identify intestinal pneumatosis (IP).

Thus, differences in height, weight, age, patient positioning, and radiographic technique were minimized among the comparisons. Only regions affected by the disease in which both radiologists agreed were evaluated by the approach.

Computational tool

A semiautomatic algorithm was developed in Matlab R2013a (Mathworks, Natick, MA, USA) for the objective evaluation of abdominal radiographs of NEC patients using different image processing methodologies. The algorithm allowed the classification of BWT and IP through FWHM measurements and wavelet-based texture analyses, respectively (Fig. 1). The two methodologies are described below. The algorithm was designed to aid radiologists to decide about the presence of abnormal BWT and IP loops.

Bowel wall thickening classification

The first methodology uses abdominal radiography (Fig. 2A) to classify BWT (Fig. 1, Method 1). The user identifies a suspicious bowel loop (black box in Fig. 2A) to be investigated further and draws a perpendicular line to the bowel wall. Normal loop (red box in Fig. 2A) is also selected in the same radiography to allow comparisons with BWT. The line size depends on the thickness of the investigated loops. The radiologist draws the line to ensure that the entire loop thickness can be evaluated.

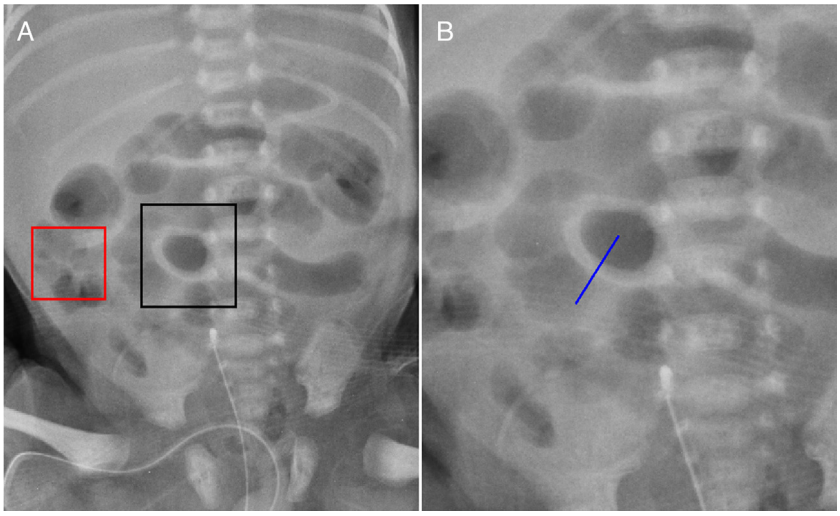

Figure 2 (A) abdominal radiography with bowel wall thickening (BWT) and normal loop circumscribed by the black box and the red box, respectively; (B) line from BWT, perpendicular to the bowel wall, identified by the radiologist.

The drawn lines for BWT and normal loops estimate a one-dimensional profile, subsequently fitted by a Gaussian function. Supplementary Fig. 2A shows the Gaussian function for the BWT represented in Fig. 2B. The FWHM, measured in millimeters, is determined over the Gaussian fit (Supplementary Fig. 2B). The FWHM measurement compares the thicknesses of BWT and normal loops.

Intestinal pneumatosis classification

The IP bowel is analyzed by wavelet transform-based texture classification (Fig. 1, Method 2). Wavelet transforms are very efficient tools for feature extraction, and they have been successfully applied to biomedical image processing.[23] After applying the wavelet transform, the resulting image is used to calculate energy. Energy contained at specific spatial frequencies and orientations can be a good indicator of texture features. This energy-based approach assumes that different texture patterns have different energy distributions in the space-frequency domain.[24] Therefore, the methodology described herein uses the combination of wavelet and energy to investigate suspicious IP loops.

The first step to analyze them is the selection of a rectangular area over the suspicious bowel loop by the user (black box in Fig. 3A). The suspicious area from the original image is extracted (Fig. 3B), thus defining a region of interest (ROI). The size of the ROI depends on the investigated loops. The radiologist selects an ROI size to ensure that the entire loop can be evaluated. To ensure that only the suspicious loop will be correctly analyzed, it is necessary to extract it from the background. Therefore, the bowel loop is segmented from the surrounding areas using a region growing technique (Fig. 3C). An ROI with normal bowel loop (red box in Fig. 3A) is also drawn and the steps described above are applied to them in the same radiograph.

A wavelet transform is applied in the segmented image (Fig. 3C). In this study, the biorthogonal transform (bio3.5) was chosen to decompose images in horizontal, vertical, and diagonal directions. When applying the wavelet transform, the approximation of the original image is also computed. The wavelet transform may be applied to many levels using the computed approximation. Fig. 4 shows an example of one level wavelet transform applied in Fig. 3C, resulting in an approximation (Fig. 4A), and decomposed images in horizontal (Fig. 4B), vertical (Fig. 4C), and diagonal (Fig. 4D) directions.

The wavelet transform was applied for eight levels. Using the decomposed images (Figs. 4B–D), the algorithm calculates the energy values of the subbands for each level[25–27] through Eq. (1).

$$Energy = \sum_{x=[p]} \sum_{x=[q]} (C(x,y))^2 \quad (1)$$

where p and q are the number of columns and rows in the ROI, respectively, and $C(x,y)$ represents the decomposed images. These energy values are compared with normal loops, thus allowing the classification of bowel loops with pneumatosis.

Comparison between suspicious and normal loops

The algorithm was evaluated in the two groups of images (BWT and IP). For both groups, regions of interest (ROIs) from normal and involved bowel loops were selected in the same radiograph by an experienced radiologist. The normal bowel loops were used as a reference, thus allowing better comparisons.

The statistical analyses of the data were performed using Minitab statistical software (MINITAB, State College, PA, USA). All of the data were nonparametric. Differences in the variables in the same image were analyzed using the paired Mann–Whitney U test. Values of $p < 0.05$ were considered statistically significance. The data are expressed as median and interquartile range.

Selection of ROIs for classification

Selection of ROIs was performed by two radiologist (S.M.R.) and (A.P.T.) with 20 and 25 years of experience in pediatric X-ray examination, and with approximately 5000 examinations reported every year. Inter-observer agreement between the two radiologists was calculated using the comparison

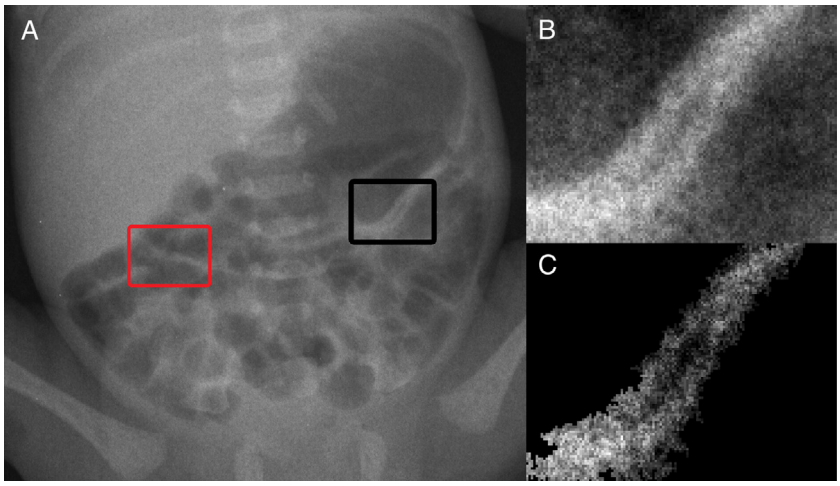

Figure 3 (A) abdominal radiograph with intestinal pneumatosis (IP) identified in the region of interest (ROI) circumscribed by the black box. Normal bowel loop is also identified in the ROI circumscribed by the red box in the same radiography; (B) highlight of ROI containing an IP-suspicious loop; (C) region of interest after segmentation of Fig. 3B based on region growing technique, which results in the extraction of the IP loop from background. ROIs, regions of interest.

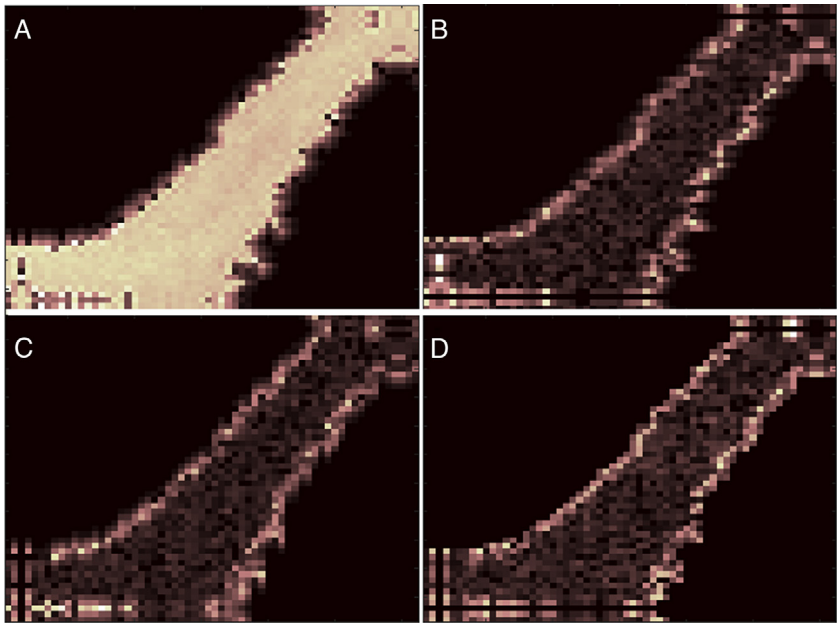

Figure 4 Results of wavelet transform application for one level. In this example, wavelet transform was applied in Fig. 3C resulting in an (A) approximation, and decomposed images in (B) horizontal, (C) vertical, and (D) diagonal directions.

between the location of selected ROIs in each X-ray exam. Furthermore, the agreement between ROI selection by the radiologists and those described in surgery reports was also calculated. Both comparisons were evaluated through Kappa inter-observer variability. This allowed to measure the degree of agreement: <0.21, 0.21–0.4, 0.41–0.6, 0.61–0.8, and 0.81–1 were considered, respectively, as poor, fair, moderate, good, and very good agreement.[28,29]

Specificity, sensitivity, and positive and negative predictive (PP and NP) values were calculated for the selected ROIs made by each radiologist, using surgery and histopathology reports as the gold standard.

Results

Bowel wall thickening assessment

The quantitative analysis of comparisons between the FWHM measurements of distended and normal loops in the BWT group showed a median of 10.30 and 15.13, respectively. The paired Mann–Whitney *U* test showed significant differences between groups ($p < 0.05$). Supplementary Fig. 3 shows boxplot comparisons of FWHM measurements of distended and normal bowel loops in the BWT group.

Intestinal pneumatosis assessment

Wavelet energy measurements of normal and IP loops were acquired in subbands for each level. The paired Mann–Whitney *U* test ($*p < 0.05$) showed that decomposition of the horizontal direction for levels seven and eight presented significant differences between normal and IP loops. For level seven, the median was 0.034 and 0.088 for normal and IP groups, respectively, and for level eight, the median was 0.19 and 0.34, respectively. No differences were found for the vertical or diagonal directions at any of the eight levels. Supplementary Fig. 4A and B show boxplot comparisons of wavelet energy measurements of the horizontal-decomposed images in levels seven and eight, respectively.

Selection of regions of interest classifications

The concordance between the surgery report and the radiologists' evaluation was analyzed by Cohen's kappa statistics. The evaluation of the presence of BWT and IP loops in the X-ray images showed that agreement between the radiologist S.M.R and the surgery report was considered excellent (BWT: $\kappa = 0.87$, IP: $\kappa = 0.85$). The agreement of the radiologist A.P.T. was considered substantial (BWT: $\kappa = 0.75$; IP: $\kappa = 0.71$). The inter-observer agreement for BWT and IP loops were considered excellent (BWT: $\kappa = 0.87$; IP: $\kappa = 0.86$).

Calculated sensibility (BWT = 0.88; IP = 1) and sensitivity (BWT = 1; IP = 0.92) of selected ROIs made by S.M.R using surgery and histopathology reports as ''gold standard'' were considered excellent, with good PP (BWT = 14; IP = 11) and NP (BWT = 14; IP = 3) values. Specificity (BWT = 0.75; IP = 1) and sensitivity (BWT = 1; IP = 0.83) values for A.P.T. were high, with good PP (BWT = 14; IP = 10) and NP (BWT = 12; IP = 3) values.

Discussion

In the present study, the authors developed a novel approach to aid the radiographic assessment of NEC in neonatal patients. The tool was applied to 50 radiographs, in which all contained normal bowel loops as a reference. The tool could detect differences in the radiographs to distinguish involved bowel loops from normal loops. These findings are important because radiographic signs are not considered completely sensitive or specific for identifying maximum risk before perforation occurs in NEC patients.[10] The interpretation of abdominal radiographs in infants can be challenging.[30]

The tool can be divided into two different image processing methodologies (Fig. 1). The first methodology is based on FWHM measurements that are able to classify bowel loops as normal and thickened. Supplementary Fig. 3 shows that the FWHM values were significantly different between normal and distended loops. This occurs because BWT is highlighted and thicker than normal loops, which can be identified based on the pixel profile.

The second methodology is based on texture analyses that can classify normal and IP bowel loops. This methodology utilizes a wavelet-based texture feature set followed by an energy distribution evaluation.[24] Horizontal, vertical, and diagonal wavelet energy measurements were evaluated at eight levels of decomposition. The horizontal direction presented sensitivity to separate normal bowel loops from bowel loops with IP involvement. Levels seven and eight in the horizontal direction presented significant differences between the extracted features (see Supplementary Fig. 4). The features of energy obtained from decomposed images adequately captured differences in NEC radiographs. Despite the fact that Supplementary Fig. 4 displays an overlap between normal and abnormal bowel, significant differences between groups were demonstrated by the paired Mann–Whitney *U* test. Therefore, this may be used by physicians as a second opinion and help them to detect normal and IP bowel loops with higher accuracy.[24]

The Cohen's kappa statistics revealed a good degree of agreement. Some discrepancies may have occurred due to the high anatomical complexity of the abdomen. This exam is performed on infants inside incubators, which can greatly reduce image quality. Despite this, there is great agreement between the report and radiologists and inter-observers, corroborating with the resulting values from Cohen's kappa statistics.

Furthermore, the values of sensitivity, specificity, and positive and negative predictive values indicated that radiologists efficiently detected IP and BWT regions. These results indicate that the selected ROIs were correctly identified and, therefore, could be used to validate the presented methodology.

Although many different imaging modalities (*e.g.*, ultrasound, magnetic resonance imaging, and computed tomography) have been investigated as diagnostic tools for NEC in the clinical setting, abdominal radiography still remains the essential and generally reliable guide for diagnosis and management of the disease.[4,10,13] Radiography, long considered the cornerstone of imaging evaluation, is widely available and relatively inexpensive, and can be performed bedside.

Determination of the clinical severity of NEC and possibly early prediction of its course are desirable objectives and may be prerequisites for successful therapy.[9] Several previous investigations evaluated the role of abdominal radiography in the diagnosis and management of NEC. However, these previous studies did not use standardized tools, such as a scale of abnormal findings, and reported poor inter- and intra-observer agreement in radiograph interpretation.[13] Wexler studied five neonates with NEC and suggested that neonates with a persistently distended loop are considered candidates for laparotomy.[31] Leonard et al. measured loops in 21 neonates with NEC and evaluated correlations between these loops and surgical indication, but no correlations were found between distended loop measurement and disease prognosis.[32] The present methodology may contribute to further studies that investigate correlations between radiological findings and disease prognosis.

According to the opinion of the observers in this study, the tool was easy to handle and particularly useful when used together with clinical findings. The authors strongly suggest that the tool should be displayed in association with the original images instead of standalone. Observers said that the use of this tool might result in reliable additional information that helps in the clinical decision, promoting a safer diagnosis.

The aim in this study was to validate this computational tool, which can possibly be used by non-experienced or non-specialist physicians to aid in the NEC diagnosis. There are some limitations in this study, as the sample size is not large, although it is compatible with other validation studies,[33–35] and the results presented here only considered cases of NEC within Bell stage 2 and 3. Although the number of radiographs is small, it should be noted that the number of regions evaluated is important. A total number of 120 regions were analyzed for BWT and 60 for IP. At a future prospective stage of the study, when the application is used in the clinical routine, other pathologies similar to NEC can

be included, as well as an association between the severities of the cases with parameters extracted from the algorithms. In addition, in this future stage, more than one pair of (compromised and healthy) loops could be evaluated per patient.

This method can be used to complement evaluations of bowel status in NEC patients, thus making management decisions easier and potentially improving patient outcome. In the future, a machine learning approach may be applied to further improve clinical applications. The present methodology should help physicians to investigate suspicious bowel loops and to predict the need for surgical intervention based on radiographs.

Conflicts of interest

The authors declare no conflicts of interest.

Acknowledgements

The authors thank all of the clinical and technical personnel at this institution's radiodiagnostic facility. The authors are also grateful to the Brazilian agencies CAPES, CNPq, and FAPESP for financial support. This work is a part of the project INCT-FNA Proc. No. 464898/2014-5.

Appendix A. Supplementary data

Supplementary data associated with this article can be found, in the online version, at doi:10.1016/j.jped.2018.05.017.

References

1. Okuyama H, Ohfuji S, Hayakawa M, Urushihara N, Yokoi A, Take H, et al. Risk factors for surgical intestinal disorders in VLBW infants: case–control study. Pediatr Int. 2016;58:34–9.
2. Lucas A, Cole TJ. Breast milk and neonatal necrotising enterocolitis. Lancet. 1990;336:1519–23.
3. Lin PW, Stoll BJ. Necrotising enterocolitis. Lancet. 2006;368:1271–83.
4. Coursey CA, Hollingsworth CL, Wriston C, Beam C, Rice H, Bisset G 3rd. Radiographic predictors of disease severity in neonates and infants with necrotizing enterocolitis. Am J Roentgenol. 2009;193:1408–13.
5. Lee JS, Polin RA. Treatment and prevention of necrotizing enterocolitis. Semin Neonatol. 2003;8:449–59.
6. He Y, Zhong Y, Yu J, Cheng C, Wang Z, Li L. Ultrasonography and radiography findings predicted the need for surgery in patients with necrotising enterocolitis without pneumoperitoneum. Acta Paediatr. 2016;105:e151–5.
7. Guthrie SO, Gordon PV, Thomas V, Thorp JA, Peabody J, Clark RH. Necrotizing enterocolitis among neonates in the United States. J Perinatol. 2003;23:278–85.
8. Buch NA, Ahmad SM, Ali SW, Hassan HM. An epidemiological study of neonatal necrotizing enterocolitis. Saudi Med J. 2001;22:231–7.
9. Leonidas JC, Hall RT. Neonatal pneumatosis coli: a mild form of neonatal necrotizing enterocolitis. J Pediatr. 1976;89:456–9.
10. Buonomo C. The radiology of necrotizing enterocolitis. Radiol Clin North Am. 1999;37:1187–98, vii.
11. Berman L, Moss RL. Necrotizing enterocolitis: an update. Semin Fetal Neonatal Med. 2011;16:145–50.
12. Epelman M, Daneman A, Navarro OM, Morag I, Moore AM, Kim JH, et al. Necrotizing enterocolitis: review of state-of-the-art imaging findings with pathologic correlation. Radiographics. 2007;27:285–305.
13. Coursey CA, Hollingsworth CL, Gaca AM, Maxfield C, Delong D, Bisset G 3rd. Radiologists' agreement when using a 10-point scale to report abdominal radiographic findings of necrotizing enterocolitis in neonates and infants. Am J Roentgenol. 2008;191:190–7.
14. Alvares BR, Martins DL, Roma RL, Pereira IM. Relevant radiological findings for the diagnosis of necrotizing enrerocolitis and its complications. Radiol Bras. 2007;40:127–30.
15. Neu J, Walker WA. Necrotizing enterocolitis. N Engl J Med. 2011;364:255–64.
16. Yee WH, Soraisham AS, Shah VS, Aziz K, Yoon W, Lee SK. Incidence and timing of presentation of necrotizing enterocolitis in preterm infants. Pediatrics. 2012;129:e298–304.
17. Zani A, Eaton S, Puri P, Rintala R, Lukac M, Bagolan P, et al. International survey on the management of necrotizing enterocolitis. Eur J Pediatr Surg. 2015;25:27–33.
18. Nino DF, Sodhi CP, Hackam DJ. Necrotizing enterocolitis: new insights into pathogenesis and mechanisms. Nat Rev Gastroenterol Hepatol. 2016;13:590–600.
19. Dong Y, Ma J. Wavelet-based image texture classification using local energy histograms. IEEE Signal Process Lett. 2011;18:247–50.
20. Bell MJ, Ternberg JL, Feigin RD, Keating JP, Marshall R, Barton L, et al. Neonatal necrotizing enterocolitis. Therapeutic decisions based upon clinical staging. Ann Surg. 1978;187:1–7.
21. Ntonfo GM, Frize M, Bariciak E. Detection of necrotizing enterocolitis in newborns using abdominal thermal signature analysis. In: 2015 IEEE International Symposium on Medical Measurements and Applications (MeMeA) Proceedings. 2015. p. 36–9.
22. Shebrya NH, Amin SK, El-Shinnawy MA, Imam SS. Abdominal ultrasonography in preterm necrotizing enterocolitis. Is it superior to plain radiography? Egypt J Radiol Nucl Med. 2012;43:457–63.
23. Annu N, Justin J. Automated classification of glaucoma images by wavelet energy features. Int J Eng Technol. 2013;5:1716–21.
24. Dua S, Acharya UR, Chowriappa P, Sree SV. Wavelet-based energy features for glaucomatous image classification. IEEE Trans Inf Technol Biomed. 2012;16:80–7.
25. Avci D, Leblebicioglu MK, Poyraz M, Dogantekin E. A new method based on Adaptive Discrete Wavelet Entropy Energy and Neural Network Classifier (ADWEENN) for recognition of urine cells from microscopic images independent of rotation and scaling. J Med Syst. 2014;38:7.
26. Sidhu S, Raahemifar K. Texture classification using wavelet transform and support vector machines. In: Canadian Conference on Electrical and Computer Engineering, Saskatoon. 2005. p. 941–4.
27. Akbarizadeh G. A New statistical-based kurtosis wavelet energy feature for texture recognition of SAR images. IEEE Trans Geosci Remote Sens. 2012;50:4358–68.
28. Landis JR, Koch GG. The measurement of observer agreement for categorical data. Biometrics. 1977;33:159–74.
29. Jacob C. A coefficient of agreement for nominal scales. Educ Psychol Meas. 1960;20:37–46.
30. Silva CT, Daneman A, Navarro OM, Moineddin R, Levine D, Moore AM. A prospective comparison of intestinal sonography and abdominal radiographs in a neonatal intensive care unit. Pediatr Radiol. 2013;43:1453–63.

31. Wexler HA. The persistent loop sign in neonatal necrotizing enterocolitis: a new indication for surgical intervention? Radiology. 1978;126:201–4.
32. Leonard T Jr, Johnson JF, Pettett PG. Critical evaluation of the persistent loop sign in necrotizing enterocolitis. Radiology. 1982;142:385–6.
33. Alves AF, Jennane R, de Miranda JR, de Freitas CC, Abdala N, de Pina DR. Ischemic stroke enhancement using a variational model and the expectation maximization method. Eur Radiol. 2018.
34. Giacomini G, Pavan AL, Altemani JM, Duarte SB, Fortaleza CM, Miranda JR, et al. Computed tomography-based volumetric tool for standardized measurement of the maxillary sinus. PLoS ONE. 2018;13:e0190770.
35. van Engeland S, Snoeren PR, Huisman H, Boetes C, Karssemeijer N. Volumetric breast density estimation from full-field digital mammograms. IEEE Trans Med Imaging. 2006;25:273–82.